Clinical Neurology and Neurosurgery 183 (2019) 105387

Contents lists available at ScienceDirect

Clinical Neurology and Neurosurgery

journal homepage: www.elsevier.com/locate/clineuro

Retrospective distortion correction of diffusion tensor imaging data by semi-elastic image fusion – Evaluation by means of anatomical landmarks

Julia Gerhardt[a], Nico Sollmann[b,c], Patrick Hiepe[d], Jan S. Kirschke[b,c], Bernhard Meyer[a], Sandro M. Krieg[a,c,*,1], Florian Ringel[a,1]

[a] Department of Neurosurgery, Klinikum rechts der Isar, Technische Universität München, Ismaninger Str. 22, 81675, Munich, Germany
[b] Department of Diagnostic and Interventional Neuroradiology, Klinikum rechts der Isar, Technische Universität München, Ismaninger Str. 22, 81675, Munich, Germany
[c] TUM-Neuroimaging Center, Klinikum rechts der Isar, Technische Universität München, Munich, Germany
[d] R&D Anatomical Mapping, Brainlab AG, Olof-Palme-Str. 9, 81829, Munich, Germany

ARTICLE INFO

Keywords:
Diffusion tensor imaging
Fiber tractography
Distortion correction
Semi-elastic image fusion
Image co-registration

ABSTRACT

Objective: Diffusion tensor imaging (DTI) based on echo-planar imaging (EPI) can suffer from geometric image distortions in comparison to conventional anatomical magnetic resonance imaging (MRI). Therefore, DTI-derived information, such as fiber tractography (FT) used for treatment planning of brain tumors, might be associated with spatial inaccuracies when linearly projected on anatomical MRI. Hence, a non-linear, semi-elastic image fusion shall be evaluated in this study that aims at correcting for image distortions in DTI.

Patients and methods: In a sample of 27 patient datasets, 614 anatomical landmark pairs were retrospectively defined in DTI and T1- or T2-weighted three-dimensional (3D) MRI data. The datasets were processed by a commercial software package (Elements Image Fusion .0; Brainlab AG, Munich, Germany) providing rigid and semi-elastic fusion functionalities, such as DTI distortion correction. To quantify the displacement prior to and after semi-elastic fusion, the Euclidian distances of rigidly and elastically fused landmarks were evaluated by means of descriptive statistics and Bland-Altman plot.

Results: For rigid and semi-elastic fusion mean target registration errors of 3.03 ± 2.29 mm and 2.04 ± 1.95 mm were found, respectively, with 91% of the evaluated landmarks moving closer to their position determined in T1- or T2-weighted 3D MRI data after distortion correction. Most efficient correction was achieved for non-superficial landmarks showing distortions up to 1 cm.

Conclusion: This study indicates that semi-elastic image fusion can be used for retrospective distortion correction of DTI data acquired for image guidance, such as DTI FT as used for a broad range of clinical indications.

1. Introduction

Diffusion tensor imaging (DTI) and fiber tractography (FT) are increasingly used in neurosurgery for pre- and intraoperative visualization of the brain's white matter (WM) anatomy in order to facilitate image-based guidance during brain tumor surgery [1–6]. In conjunction with neurophysiological functional mapping, such as navigated transcranial magnetic stimulation, consideration of subcortical fiber pathways may improve the extent of resection and simultaneously reduce postoperative deficit rates [7–12]. In order to have FT information available in standard image space used for image-guided surgery the DTI volume has to be co-registered to conventional anatomical, three-dimensional (3D) magnetic resonance imaging (MRI) data [13,14].

Rigid co-registration of 3D T1-weighted MRI and DTI data represents the standard procedure to fuse anatomical and FT information [3,14]. This linear co-registration approach allows translation and rotation in 3D space, i.e. in six degrees of freedom (DOF), and thus is only reliable if the geometry of the imaged anatomical structures appear exactly the same in both datasets.

Due to the application of the ultra-fast echo-planar imaging (EPI) technique in DTI the derived diffusion metrics and reconstructed WM fiber representations are inherently prone to non-rigid geometric

Abbreviations: 3D, three-dimensional; DOF, degrees of freedom; DTI, diffusion tensor imaging; EPI, echo-planar imaging; FLAIR, fluid-attenuated inversion recovery; FT, fiber tractography; MRI, magnetic resonance imaging; SD, standard deviation; TRE, target registration error; WM, white matter

* Corresponding author at: Department of Neurosurgery, Klinikum rechts der Isar, Technische Universität München, Ismaninger Str. 22, 81675, Munich, Germany.
E-mail addresses: julegerhardt@web.de (J. Gerhardt), Nico.Sollmann@tum.de (N. Sollmann), Patrick.Hiepe@brainlab.com (P. Hiepe), Jan.Kirschke@tum.de (J.S. Kirschke), Bernhard.Meyer@tum.de (B. Meyer), Sandro.Krieg@tum.de (S.M. Krieg), Florian.Ringel@unimedizin-mainz.de (F. Ringel).

[1] Both authors contributed equally to this work.

https://doi.org/10.1016/j.clineuro.2019.105387
Received 22 April 2019; Received in revised form 4 June 2019; Accepted 10 June 2019
Available online 10 June 2019
0303-8467/

distortions. Such distortions are non-systematic and patient-specific, thus cannot be corrected directly by the MRI scanner system. Therefore, many distortion correction methods have been proposed previously, which are based on advanced reconstruction techniques using magnetic field mapping [15], point-spread-function mapping [16], or forward-reverse trajectory EPI acquisition [17–19]. These approaches rely on non-linear, deformable image co-registration (i.e., elastic image fusion with more than six DOF), which can optimize the intra-modal image alignment even in areas with strong geometric distortions [18,19].

However, since these approaches commonly require additional scan time, retrospective distortion correction methods have been suggested, which, in essence, allow spatially aligning DTI data with respect to standard anatomical MRI data without requiring additional MRI data acquisition [20–23]. Such inter-modal non-linear image co-registration methods incorporate dedicated cost functions penalizing undesired image deformations. These methods, however, still show high prevalence of local image co-registration artifacts, which currently prevent their establishment in the clinical routine.

The aim of the present work is to exploit a novel, commercially available semi-elastic fusion approach (Elements Distortion Correction Cranial4.0; Brainlab AG, Munich), which may enable retrospective, fully automated and reliable distortion correction of DTI data and thus facilitate FT applications in clinical settings. We hypothesize that the proposed method improves the image co-registration accuracy of representative clinical T1- and T2-weighted MRI and DTI data in a cohort of patients suffering from intracranial tumors or psychiatric disorders. The co-registration accuracy is quantified via Euclidean distance measurements of landmarks related to anatomical structures. The target registration error (TRE) is evaluated and statistically compared for rigid and semi-elastic fusion of clinically representative imaging fusion scenarios.

2. Materials and methods

2.1. Ethics

This retrospective, single-center study was approved by the local institutional review board (registration number: 545/16S) and was carried out in accordance with the ethical standards of the Declaration of Helsinki and its later amendments. The local institutional review board waived the requirement to obtain patient informed consent due to the retrospective design of the study.

2.2. Patients and scans

Retrospective, anonymized patient datasets of 27 patients with eloquent high-grade glioma ($n_1 = 8$), low-grade glioma ($n_2 = 5$), meningioma of the skull base ($n_3 = 4$) or in eloquent areas ($n_4 = 5$), or psychiatric disorders ($n_5 = 5$) were included in this evaluation (Table 1). Lesion volumes varied from approximately 2 cm^3 to 169 cm^3 and were located in different regions of the brain. The patient datasets comprised a DTI scan acquired by means of EPI and either a 3D T1-weighted gradient-echo sequence or a 3D fluid-attenuated inversion recovery (FLAIR) sequence. In detail, DTI data were retrospectively corrected with respect to 3D T1-weighted MRI scans with contrast agent ($n_{T1wCA\text{-}B0}$) or without contrast agent ($n_{T1wMR\text{-}B0}$) as well as based on 3D FLAIR data ($n_{T2wMR\text{-}B0}$). Mean in- and through-plane resolution of conventional reference MRI data were 0.79 ± 0.24 mm and 1.16 ± 1.52 mm, respectively. The evaluated DTI data showed an in- and through-plane resolution of 1.43 ± 0.46 mm and 3.13 ± 1.61 mm, respectively.

2.3. Distortion correction method

All images were retrospectively processed using Elements Image Fusion .0 (Brainlab AG, Munich, Germany) including the applications Elements Rigid Image Fusion .0 and Elements Distortion Correction Cranial .0 for rigid and semi-elastic image co-registration, respectively. For both procedures, the DTI-derived B0 images were fused to conventional anatomical MRI data.

In a first step, inter-modal rigid fusion of DTI and conventional anatomical MRI was performed using a mutual information-based linear co-registration algorithm [24]. Afterwards, Elements Distortion Correction Cranial 4.0 was used to elastically deform the geometrically distorted B0 images with respect to the reference scan (Figs. 1 and 2). Therefore, image segmentation considering voxel-wise anatomic labeling of the 3D MRI was automatically performed by means of a Synthetic Tissue Model (patent WO 2014063840 A1), and the image volume related to the brain was subdivided into $3 \times 3 \times 3\ cm^3$ image volumes. Semi-elastic image fusion was performed by calculating multiple affine co-registrations for each 3D sub-volume and ultimately determining a 3D deformation vector field by interpolation of the local affine co-registration estimates. Here, the 3D deformation field described the pixel-wise morphing of the B0 image volume in order to spatially align it with respect to the 3D reference MRI scan.

2.4. Anatomical landmarks and evaluation of distortion correction

Quantitative evaluation of the proposed method was conducted by Euclidian distance measurements between landmarks of identical anatomical structures for rigidly and semi-elastically fused image data. Therefore, Elements DICOM Viewer 4.0 (Brainlab AG, Munich, Germany) was used to determine corresponding label points in the DTI-B0 and reference 3D MRI scan. These landmarks were defined in multiplanar reconstructions of both scans and distributed almost evenly throughout the brain. On average, for each patient dataset 23 landmark pairs were defined in the reference and distorted image volume. Automatic post-processing routines were used to measure the target registration error for rigid fusion (TRE_{rigid}) and semi-elastic fusion ($TRE_{elastic}$).

2.5. Statistical analyses

Data analyses and descriptive statistics were conducted using MATLAB (MathWorks, Natick, USA). All TRE values are given in mean ± standard deviation (SD). Gaussian distribution of quantities was tested by Kolmogorov-Smirnov tests. A p-value of < 0.05 was considered statistically significant. Statistical differences of TRE_{rigid} and $TRE_{elastic}$ values were assessed via Wilcoxon rank-sum tests. Correlation and Bland-Altman analyses of TRE_{rigid} and $TRE_{elastic}$ values were performed in order to assess the effectiveness of the proposed method depending on initial displacement shown by the reference method (rigid fusion as quantified by TRE_{rigid}). Graphical analysis and Spearman correlations were used to identify linear relationships between spatial resolution of fused images and the image fusion accuracy after distortion correction (quantitation by $TRE_{elastic}$). In addition, average values of patient-specific mean and maximum TRE_{rigid} and $TRE_{elastic}$ values were determined for different lesion types, locations, and seizure status.

3. Results

In total, 614 landmarks were evaluated in 27 fusion pairs showing mean TRE values of 3.03 ± 2.29 mm and 2.04 ± 1.95 mm for rigid and semi-elastic fusion, respectively (Table 2). Thus, the proposed DTI distortion correction method resulted in an improvement of the image fusion accuracy by 1.0 ± 1.0 mm on average. As illustrated in Fig. 3, correlation and regression analyses between TRE values for rigid fusion (TRE_{rigid}) and after distortion correction ($TRE_{elastic}$) showed that the vast majority, i.e. 91% of the data points, are located below the line-of-identity with a significant regression coefficient of $r = 0.902$ ($p < 0.001$) with a slope of 0.77. Correspondingly, 9% of the

Table 1
Properties of investigated fusion scenarios.

Clinical indication	Combined modalities	In-plane resolution of reference image (in mm)	Slice distance of reference image (in mm)	In-plane resolution of distorted image (in mm)	Slice distance of distorted image (in mm)	Tumor size (in cm^3)	Tumor location	Mean TRE_{rigid} (in mm)	Mean $TRE_{elastic}$ (in mm)	Maximum TRE_{rigid} (in mm)	Maximum $TRE_{elastic}$ (in mm)
High-grade	T1wCA-B0	0.80	0.80	1.80	5.20	62.90	frontal	2.26	1.85	3.92	3.55
Glioma	T1wCA-B0	0.94	1.00	0.88	2.00	31.30	temporal	2.36	1.78	5.33	3.58
Typical workflow:	T1wCA-B0	0.90	1.00	0.88	2.00	2.48	motor	3.71	2.82	9.73	9.67
cranial planning and	T1wCA-B0	0.98	1.00	0.88	2.00	26.10	temporal	3.88	2.94	19.50	17.42
stereotactic	T1wMR-B0	0.90	1.00	1.75	2.00	39.80	occipital	4.36	3.38	14.84	12.56
procedures	T2wMR-B0	0.40	0.60	1.75	2.00	58.60	occipital	4.33	3.22	13.42	12.21
	T1wCA-B0	0.91	1.00	0.88	2.00	168.90	temporal	3.27	2.21	12.62	8.91
	T1wMR-B0	0.49	1.00	1.72	2.00	107.50	frontal	4.36	3.28	16.03	13.40
Low-grade	T1wMR-B0	0.80	1.50	1.72	6.50	0.65	frontal	4.03	2.72	10.77	9.39
Glioma	T1wMR-B0	1.00	1.00	0.86	3.00	20.40	parietal	2.03	1.42	3.91	2.65
Typical workflow:	T1wCA-B0	0.94	1.00	0.88	2.00	32.30	frontal	2.91	1.79	7.86	5.78
cranial planning and	T1wCA-B0	0.50	1.00	0.86	3.00	19.00	frontal	3.18	2.05	10.63	7.29
stereotactic	T2wMR-B0	0.50	2.00	0.86	3.00	25.80	frontal	3.36	1.67	10.47	6.68
procedures											
Meningioma of the	T1wCA-B0	0.44	1.00	1.15	4.40	2.02	skull base	3.46	1.90	11.78	7.80
skull base	T1wMR-B0	0.48	1.00	1.95	2.60	2.53	skull base	2.01	1.30	3.77	2.41
Typical workflow:	T1wMR-B0	0.48	1.00	1.95	2.60	17.90	skull base	2.28	1.86	9.71	8.45
cranial planning	T1wMR-B0	1.00	1.00	1.20	6.50	2.54	skull base	2.58	1.97	12.03	11.03
procedures											
Meningioma in	T1wMR-B0	1.00	1.00	1.50	3.75	24.90	parietal	1.66	1.13	4.61	2.67
eloquent areas	T1wMR-B0	1.00	1.00	1.60	1.60	30.90	parietal	2.35	1.30	5.68	5.72
Typical workflow:	T1wMR-B0	1.00	1.00	1.60	1.60	21.50	motor	2.66	1.59	4.86	4.00
cranial planning	T1wMR-B0	1.00	1.00	2.05	2.60	21.30	motor	2.11	1.76	7.25	7.07
procedures	T2wMR-B0	0.45	3.30	2.05	2.60	23.50	motor	1.90	1.40	8.39	7.97
Cases for deep brain	T1wMR-B0	0.53	2.00	1.80	3.00	–	–	2.65	1.92	8.41	7.65
stimulation	T1wMR-B0	1.00	1.00	1.20	6.50	–	–	2.65	1.73	8.02	6.20
Typical workflow:	T1wMR-B0	1.00	1.00	2.00	2.00	–	–	3.96	1.82	8.05	4.32
stereotactic	T2wMR-B0	1.00	1.00	2.00	2.00	–	–	4.36	2.07	8.78	6.59
procedures	T1wCA-B0	0.94	1.20	0.94	6.00	–	–	2.61	1.57	4.32	3.58

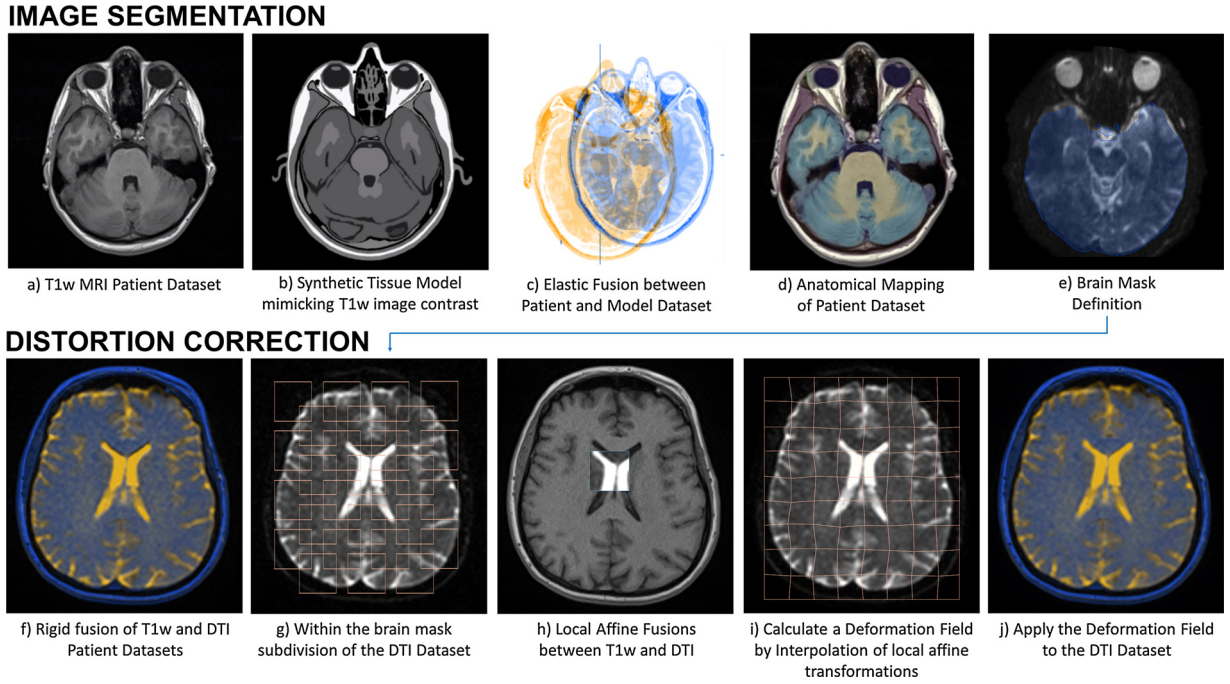

Fig. 1. Principles of semi-elastic fusion.
This figure shows the steps performed for semi-elastic fusion, including image segmentation and distortion correction.

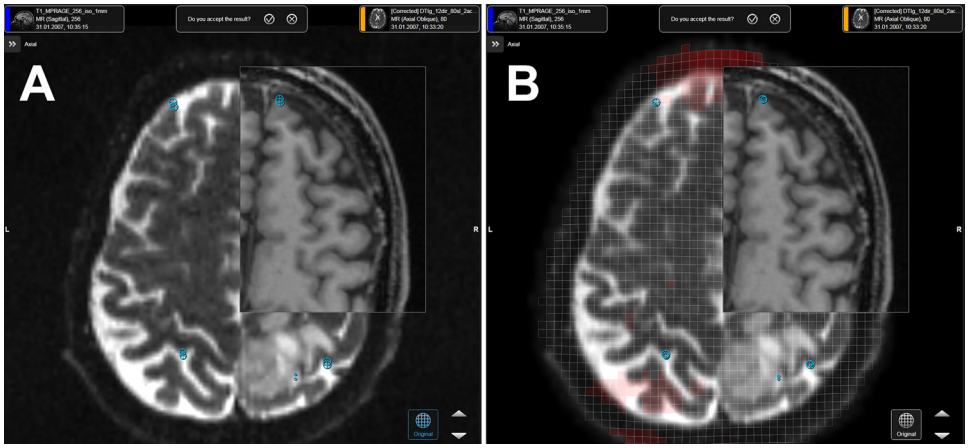

Fig. 2. Example of semi-elastic fusion for distortion correction.
Rigid fusion (A) and semi-elastic fusion (B) for one fusion pair consisting of diffusion tensor imaging (DTI) and conventional anatomical magnetic resonance imaging (MRI) data. The heat map shown onto the semi-elastic fusion (B) highlights areas where the highest fraction of non-linear deformation was applied by the fusion method. In this case, the B0 image was stretched in order to achieve alignment with the anatomical MRI data.

Table 2
Target registration error (TRE) for rigid fusion (TRE_{rigid}) and semi-elastic fusion ($TRE_{elastic}$).

	TRE_{rigid}	$TRE_{elastic}$	p-value
TRE (in mm)	3.03 ± 2.29	2.04 ± 1.95	< 0.001
Median / 95% quantile (in mm)	2.39 / 7.47	1.43 / 5.39	–

landmarks showed an increase of TRE due to semi-elastic image fusion.

The Bland-Altman plot illustrates statistical agreement between both methods by plotting the individual differences of rigid and semi-elastic fusion accuracy measurements, i.e. TRE_{rigid} and $TRE_{elastic}$, allowing to assess the differences dependent on the reference procedure (quantified via TRE_{rigid}; Fig. 3). It shows non-symmetric, negatively skewed (Kolmogorov-Smirnov test: $p < 0.001$; skewness = -1.3) and systematically scaled differences (scaled by TRE_{rigid}) with a significant bias of -1.0 mm (rank sum test: $p < 0.001$; with a coefficient of reproducibility of 2 mm corresponding to 1.96 times the SD of the difference).

The 95% limits-of-agreement (95% confidence interval given by average difference ± 1.96 SD) were 0.96 mm and -3.0 mm, indicating that after semi-elastic fusion 95% of the label points yield up to 0.96 mm higher and down to 3 mm lower TRE values than compared to rigid fusion, respectively. Beyond the 95% limits-of-agreement the vast majority of individual estimates showing significant disagreements are attributable to negative differences between TRE_{rigid} and $TRE_{elastic}$, and thus to increased image fusion accuracy due to application of the proposed method. Positive differences (i.e., 9% of evaluated landmarks) were found for $TRE_{rigid} < 5$ mm (except of one landmark at $TRE_{rigid} = 6.5$ mm) Statistically significant negative differences (below -3.0 mm) are mainly given for TRE_{rigid} in the range of approximately 4–13 mm.

Further analyses showed that highest mean and maximum TRE_{rigid} and $TRE_{elastic}$ were found for patients with high-grade gliomas (followed by low-grade gliomas and meningioma of the skull base) and lesions in the occipital area (followed by frontal, temporal, and skull base area). DTI data of patients without space-occupying lesions showed lower but comparable registration errors. Contrary, no clear associations between tumor size and TRE estimates were found (Table 1). In addition, no relationship between spatial resolution and TRE estimates were found through graphical analysis.

4. Discussion

The present study indicates that the proposed method for retrospective correction of geometric image distortions in DTI datasets by means of semi-elastic image fusion is capable of significantly improving the image fusion accuracy between DTI and conventional anatomical MRI data. The method thus can be used to correct FT data in the future and to compensate for geometric inaccuracies of reconstructed WM representations potentially critical for image-guided surgery near functional areas.

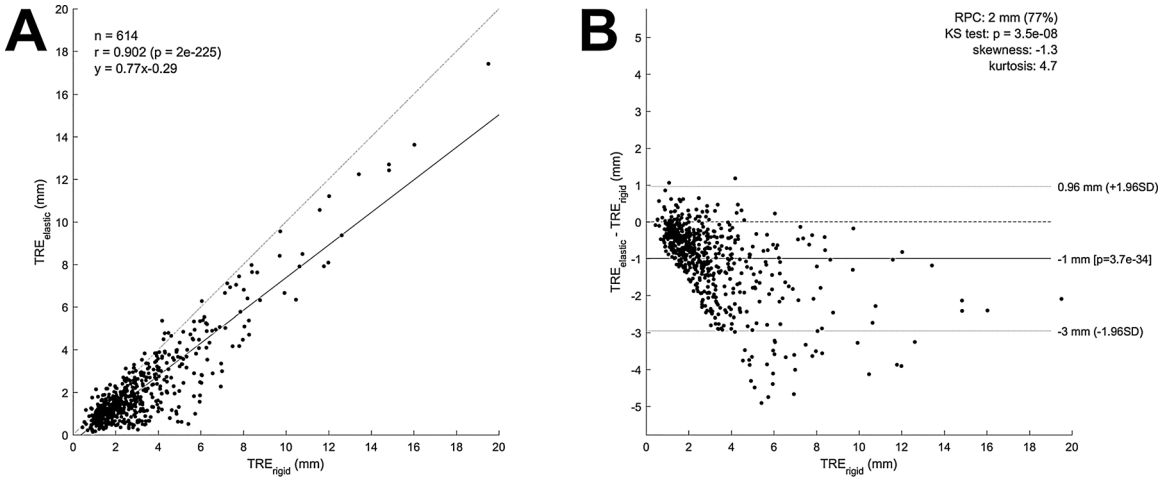

Fig. 3. Results of target registration error (TRE) measurements.
Regression analysis (A) and Bland-Altman plot (B) of the TRE for rigidly fused (TRE_{rigid}) and semi-elastically fused ($TRE_{elastic}$) data.

4.1. Technical aspects

Susceptibility artifacts inherent to EPI data cause spatial distortions of DTI-derived fiber tracts when using linear, rigid image co-registration techniques [15]. Previously, it was shown that these inaccuracies may be up to several millimeters and correction methods are a prerequisite when integrating FT into a stereotactic setup for intraoperative guidance [5,23]. For instance, by using a landmark-based evaluation approach mean co-registration inaccuracies for the pyramidal tract in anterior-posterior direction of 4.0 ± 2.8 mm, 2.4 ± 1.7 mm, and 3.2 ± 3.5 mm were found in the area of the cortex, internal capsule, and brainstem, respectively [5]. In the present study a mean TRE_{rigid} of 3.03 ± 2.29 mm was found showing a 95% confidence interval of 7.47 mm throughout the brain of 27 patient datasets with highest displacements in occipital, frontal, temporal, and skull base areas. Correspondingly, human studies have shown that in superficial regions (adjacent to air-bone / bone-brain border regions, like frontal lobes or brainstem) image distortions can account for up to 15–20 mm, and that it is clinically important to characterize and remove substantial distortions [23]. In this study the effect was found to be rather independent on the lesion type and seizure status (Table 1).

By application of the proposed semi-elastic image fusion approach a significant reduction of the TRE was achieved, leading to an image co-registration accuracy of $TRE_{elastic}$ = 2.04 ± 1.95 mm with median and 95% quantile values of 1.43 mm and 5.39 mm, respectively. Similar results have been reported with misalignments after non-linear fusion in the range of 1–2 mm [5,23]. The authors further interpreted these results in light of the spatial image resolution, which was approximately 2 mm^3. However, it remained unclear whether the spatial resolution is associated with resulting fusion accuracies.

In the present study, the evaluated DTI data showed a mean slice resolution of 3.13 ± 1.61 mm with a maximum sampling rate of 6.5 mm. As indicated by the Bland-Altman plot (Fig. 3), higher TRE values after semi-elastic fusion ($TRE_{elastic} > TRE_{rigid}$) were only present for distortions below 6.5 mm (TRE_{rigid}). Thus, it can be argued that lower spatial resolution result in increased uncertainty during (1) the manual landmark definition and (2) the process of semi-elastic fusion itself (e.g., re-gridding artifacts). However, no linear association between TRE after semi-elastic fusion and the spatial resolution was found in this work. Therefore, future studies are required to investigate the relationship between fusion accuracy and spatial characteristics of fusion data.

In addition, the lower correction magnitude reported in this study compared to the literature might be related to inherent limitations of the semi-elastic fusion approach. Since this approach is designed to compensate for large scale distortions (with low frequency such as extending over the entire field of view) it is inherently limited when it comes to compensation of very large, local distortions. This is supported by the presented results, where significant TRE reductions (i.e., differences between $TRE_{elastic}$ and TRE_{rigid} below the 95% limits of agreement) were mainly found for distortions in the range of 4–13 mm (TRE_{rigid}), while at higher TRE_{rigid} values the correction rate was less prominent (Fig. 3). Together with the uncertainty at very low TRE_{rigid} values (due to limited spatial resolution), this may lead to lower improvements assessable after semi-elastic fusion. In the future, more DOF during non-linear co-registration, such as available by diffeomorphic, fully elastic fusion, may facilitate compensation of high frequency distortions [23]. However, the notion of the proposed semi-elastic fusion method was to provide a robust retrospective distortion correction method applicable for clinical routine, where less prevalence rates of local deformation artifacts is desired.

4.2. Clinical considerations

DTI-based FT has become an important part of pre- and intraoperative neuronavigation, although being intrinsically prone to registration inaccuracies due to geometric image distortions. Inaccuracies of 3 mm, on average, and up to 20 mm, as assessed in this study, can be regarded as clinically relevant depending on the surgical procedure. For instance, studies on intraoperative subcortical stimulation suggest tumor resection up to 1–3 mm adjacent to the corticospinal tract [25]. With regard to the intraoperatively observed brain shift, the geometric distortions can potentially affect the surgical outcome when operating on subcortical eloquent lesions [26–28]. In addition, in the context of stereotactic interventions, such as performed for deep brain stimulation and in epilepsy surgery, distortion correction of FT data might be crucial for desired clinical outcome [29,30]. In the future, a similar semi-elastic fusion approach like presently introduced can be also used to correct mild surgery-induced brain shifts (approximately 3–5 mm) like observed during implantation of subdural electrodes, for instance [31].

5. Conclusion

In this work we evaluated a semi-elastic image fusion approach designed for retrospective correction of geometric image distortion routinely observed in DTI. The representative data pool showed that semi-elastic fusion significantly increases the image fusion accuracy of DTI and conventional anatomical 3D MRI fusion scenarios. Landmark distance measurements yielded that distortions up to 1 cm can be efficiently reduced to approximately 2 mm, on average, which might be critical for many surgical interventions relying on image-guidance and DTI-based FT of the brain's WM anatomy.

Declarations of interest

BM, SK, and FR are consultants for Brainlab AG (Munich, Germany). PH is employed by Brainlab AG (Munich, Germany). SK is consultant for Nexstim Plc (Helsinki, Finland), NS received honoraria from Nexstim Plc (Helsinki, Finland). The study was financed by institutional grants from the Department of Neurosurgery.

Data statement

The raw data that support the findings of this study are available from the corresponding author upon reasonable request.

Acknowledgement

Not applicable.

References

[1] A. Castellano, L. Bello, C. Michelozzi, M. Gallucci, E. Fava, A. Iadanza, M. Riva, G. Casaceli, A. Falini, Role of diffusion tensor magnetic resonance tractography in predicting the extent of resection in glioma surgery, Neuro Oncol. 14 (2) (2012) 192–202.

[2] C.A. Clark, T.R. Barrick, M.M. Murphy, B.A. Bell, White matter fiber tracking in patients with space-occupying lesions of the brain: a new technique for neurosurgical planning? Neuroimage 20 (3) (2003) 1601–1608.

[3] S. Farquharson, J.D. Tournier, F. Calamante, G. Fabinyi, M. Schneider-Kolsky, G.D. Jackson, A. Connelly, White matter fiber tractography: why we need to move beyond DTI, J. Neurosurg. 118 (6) (2013) 1367–1377.

[4] S. Garcia, J. Rincon-Torroella, A. Benet, L. Oleaga, J.J. Gonzalez Sanchez, Assessment of white matter transgression during neuroendoscopic procedures using diffusion tensor image fiber tracking, World Neurosurg. 99 (2017) 232–240.

[5] D. Merhof, G. Soza, A. Stadlbauer, G. Greiner, C. Nimsky, Correction of susceptibility artifacts in diffusion tensor data using non-linear registration, Med. Image Anal. 11 (6) (2007) 588–603.

[6] M. Yoshino, K. Abhinav, F.C. Yeh, S. Panesar, D. Fernandes, S. Pathak, P.A. Gardner, J.C. Fernandez-Miranda, Visualization of cranial nerves using high-definition fiber tractography, Neurosurgery 79 (1) (2016) 146–165.

[7] C. Negwer, E. Beurskens, N. Sollmann, S. Maurer, S. Ille, K. Giglhuber, J.S. Kirschke, F. Ringel, B. Meyer, S.M. Krieg, Loss of subcortical language pathways correlates with surgery-related aphasia in patients with brain tumor: an investigation via repetitive navigated transcranial magnetic stimulation-based diffusion tensor imaging fiber tracking, World Neurosurg. 111 (2018) e806–e818.

[8] C. Negwer, S. Ille, T. Hauck, N. Sollmann, S. Maurer, J.S. Kirschke, F. Ringel, B. Meyer, S.M. Krieg, Visualization of subcortical language pathways by diffusion tensor imaging fiber tracking based on rTMS language mapping, Brain Imaging Behav. 11 (3) (2017) 899–914.
[9] T. Picht, D. Frey, S. Thieme, S. Kliesch, P. Vajkoczy, Presurgical navigated TMS motor cortex mapping improves outcome in glioblastoma surgery: a controlled observational study, J. Neurooncol. 126 (3) (2016) 535–543.
[10] C. Weiss, I. Tursunova, V. Neuschmelting, H. Lockau, C. Nettekoven, A.M. Oros-Peusquens, G. Stoffels, A.K. Rehme, A.M. Faymonville, N.J. Shah, K.J. Langen, R. Goldbrunner, C. Grefkes, Improved nTMS- and DTI-derived CST tractography through anatomical ROI seeding on anterior pontine level compared to internal capsule, Neuroimage Clin. 7 (2015) 424–437.
[11] S.M. Krieg, N. Sollmann, T. Obermueller, J. Sabih, L. Bulubas, C. Negwer, T. Moser, D. Droese, T. Boeckh-Behrens, F. Ringel, B. Meyer, Changing the clinical course of glioma patients by preoperative motor mapping with navigated transcranial magnetic brain stimulation, BMC Cancer 15 (2015) 231.
[12] N. Sollmann, S. Ille, T. Hauck, S. Maurer, C. Negwer, C. Zimmer, F. Ringel, B. Meyer, S.M. Krieg, The impact of preoperative language mapping by repetitive navigated transcranial magnetic stimulation on the clinical course of brain tumor patients, BMC Cancer 15 (1) (2015) 261.
[13] B. Jeurissen, M. Descoteaux, S. Mori, A. Leemans, Diffusion MRI fiber tractography of the brain, NMR Biomed. 32 (April (4)) (2019) e3785, https://doi.org/10.1002/nbm.3785 Epub 2017 Sep 25.
[14] T. Schultz, A. Vilanova, Diffusion MRI visualization, NMR Biomed. 32 (April (4)) (2019) e3902, https://doi.org/10.1002/nbm.3902 Epub 2018 Feb 27.
[15] P. Jezzard, R.S. Balaban, Correction for geometric distortion in echo planar images from B0 field variations, Magn. Reson. Med. 34 (1) (1995) 65–73.
[16] M.H. In, O. Posnansky, E.B. Beall, M.J. Lowe, O. Speck, Distortion correction in EPI using an extended PSF method with a reversed phase gradient approach, PLoS One 10 (2) (2015) e0116320.
[17] M.O. Irfanoglu, P. Modi, A. Nayak, E.B. Hutchinson, J. Sarlls, C. Pierpaoli, DR-BUDDI (Diffeomorphic Registration for Blip-Up blip-Down Diffusion Imaging) method for correcting echo planar imaging distortions, Neuroimage 106 (2015) 284–299.
[18] D. Holland, J.M. Kuperman, A.M. Dale, Efficient correction of inhomogeneous static magnetic field-induced distortion in Echo Planar Imaging, Neuroimage 50 (1) (2010) 175–183.
[19] L. Ruthotto, H. Kugel, J. Olesch, B. Fischer, J. Modersitzki, M. Burger, C.H. Wolters, Diffeomorphic susceptibility artifact correction of diffusion-weighted magnetic resonance images, Phys. Med. Biol. 57 (18) (2012) 5715–5731.
[20] C. Bhushan, J.P. Haldar, S. Choi, A.A. Joshi, D.W. Shattuck, R.M. Leahy, Co-registration and distortion correction of diffusion and anatomical images based on inverse contrast normalization, Neuroimage 115 (2015) 269–280.
[21] P. Liu, B. Eberhardt, C. Wybranski, J. Ricke, L. Ludemann, Nonrigid 3D medical image registration and fusion based on deformable models, Comput. Math. Methods Med. 2013 (2013) 902470.
[22] H. Rivaz, Z. Karimaghaloo, D.L. Collins, Self-similarity weighted mutual information: a new nonrigid image registration metric, Med. Image Anal. 18 (2) (2014) 343–358.
[23] H. Huang, C. Ceritoglu, X. Li, A. Qiu, M.I. Miller, P.C. van Zijl, S. Mori, Correction of B0 susceptibility induced distortion in diffusion-weighted images using large-deformation diffeomorphic metric mapping, Magn. Reson. Imaging 26 (9) (2008) 1294–1302.
[24] J.F. Daisne, A. Blumhofer, Atlas-based automatic segmentation of head and neck organs at risk and nodal target volumes: a clinical validation, Radiat. Oncol. 8 (2013) 154.
[25] A. Raabe, J. Beck, P. Schucht, K. Seidel, Continuous dynamic mapping of the corticospinal tract during surgery of motor eloquent brain tumors: evaluation of a new method, J. Neurosurg. 120 (5) (2014) 1015–1024.
[26] M.H. Reinges, T. Krings, H.H. Nguyen, F.J. Hans, M.C. Korinth, M. Holler, W. Kuker, R. Thiex, U. Spetzger, J.M. Gilsbach, Is the head position during preoperative image data acquisition essential for the accuracy of navigated brain tumor surgery? Comput. Aided Surg. 5 (6) (2000) 426–432.
[27] O. Suess, T. Kombos, O. Ciklatekerlio, R. Stendel, S. Suess, M. Brock, Impact of brain shift on intraoperative neurophysiological monitoring with cortical strip electrodes, Acta Neurochir. (Wien) 144 (12) (2002) 1279–1289 discussion 1289.
[28] P. Hastreiter, C. Rezk-Salama, G. Soza, M. Bauer, G. Greiner, R. Fahlbusch, O. Ganslandt, C. Nimsky, Strategies for brain shift evaluation, Med. Image Anal. 8 (4) (2004) 447–464.
[29] N. Vanegas-Arroyave, P.M. Lauro, L. Huang, M. Hallett, S.G. Horovitz, K.A. Zaghloul, C. Lungu, Tractography patterns of subthalamic nucleus deep brain stimulation, Brain 139 (Pt 4) (2016) 1200–1210.
[30] V.A. Coenen, N. Allert, S. Paus, M. Kronenburger, H. Urbach, B. Madler, Modulation of the cerebello-thalamo-cortical network in thalamic deep brain stimulation for tremor: a diffusion tensor imaging study, Neurosurgery 75 (6) (2014) 657–669 discussion 669-70.
[31] L.H. Stieglitz, C. Ayer, K. Schindler, M.F. Oertel, R. Wiest, C. Pollo, Improved localization of implanted subdural electrode contacts on magnetic resonance imaging with an elastic image fusion algorithm in an invasive electroencephalography recording, Neurosurgery 10 (Suppl 4) (2014) 506–512 discussion 512-3.